C00-3130-TB-211
Conf-740610--1
Conf-740713--42

Submitted to:

Symposium on Antinucleon-Nucleon Interactions
Prague, Czechoslovakia
24-28 June 1974

and

XVII International Conference on High Energy Physics
Imperial College, London
1-10 July 1974

# Angular Distributions of $\bar{p}p \to \pi^\circ\pi^\circ$ and $\bar{p}p \to \pi^\circ\eta^\circ$ at 1.752 GeV/c*


C. DeMarzo, L. Guerriero, F. Posa, E. Vaccari, F. Waldner
Bari University, Italy†

R. E. Lanou (Jr.), J. T. Massimo, R. K. Thornton
Brown University, Providence, R.I. 02912 U.S.A.††

D. S. Barton, B. A. Nelson, M. Marx, D. C. Peaslee§, L. Rosenson
Massachusetts Institute of Technology and
Laboratory for Nuclear Science
Cambridge, Mass. 02139 U.S.A.††



## ABSTRACT

An experiment has been performed to measure the angular distributions in the reactions $\bar{p}p \to \pi^\circ\pi^\circ$ and $\to \pi^\circ\eta^\circ$ at an incident $\bar{p}$ momentum of 1.752 GeV/c. Structure is seen in the angular distributions for both reactions. These data are combined with those of Eisenhandler et al. on $\bar{p}p \to \pi^+\pi^-$ to determine the angular distributions in the states $I^G = 0^+$ and $I^G = 1^+$; pronounced structure is seen in both states which differ significantly from that of $\pi^\circ\eta^\circ$ ($I^G = 1^-$).


*Part of this work has been carried out at the Brookhaven National Laboratory, Upton, New York 11973 U.S.A.


†Work supported by the USA-Italy Scientific Cooperation Program and the Istituto Nazionale di Fisica Nucleare

††Work supported by the U.S. Atomic Energy Commission under Contracts # AT(11-1)-3130TB and AT(11-1)-3069



§Permanent address: Australian National University
Canberra, Australia


MASTER

## DISCLAIMER

We present here preliminary results of an optical spark chamber experiment to measure gamma ray final states of proton-antiproton annihilations. Angular distributions are given for $\bar{p}p \to \pi^\circ\pi^\circ$ and $\bar{p}p \to \pi^\circ\eta^\circ$ at 1.752 GeV/c incident momentum.

The experiment was performed in a partially separated antiproton beam at the Brookhaven National Laboratory AGS. The beam included two 15 foot D.C. separators and a 12 element tagging hodoscope at the momentum focus, giving us a momentum resolution capability of 0.4%. After separation the beam contained equal numbers of $\bar{p}$ and $\pi^-$. Using a 16 meter flight path we were able to achieve better than a $10^{-3}$ rejection rate of pions. The beam was then incident on a 10 cm liquid hydrogen target which was surrounded by a two layer scintillation counter hodoscope covering the entire solid angle. The first layer vetoed all events with charged secondaries. Between the layers was one radiation length of lead in order to convert gamma rays. The second layer consisted of 17 counters designed to be sensitive to two body correlations. A good trigger was required to have a count in two counters - one forward, one backward, and on the same azimuth (Fig. 1). This strongly biased our trigger against the neutral baryonic reactions like $\bar{n}n$ and $\bar{n}n\pi^\circ$, and towards two body states like $\pi^\circ\pi^\circ$ and $\pi^\circ\eta^\circ$. For example, the $\bar{n}n$ triggering efficiency was $\simeq 10^{-3}$ while that for $\pi^\circ\pi^\circ$ was $\simeq 0.4$. If an event satisfied the logic we then fired the spark chambers.

The six spark chambers covered the entire solid angle and presented a minimum of eight radiation lengths in 80 gaps for converting and detecting the gamma ray showers (Fig. 2). The upstream chamber had a hole through its plates to admit the beam, with foil over the first few and last few gaps, to permit measurement of the incoming track. Each spark chamber was photographed in two 90° stereo views. In addition two small thin foil chambers just before and after the target permitted identification of non-target interactions and considerably improved the beam track determination. Also recorded on the film was information about the momentum hodoscope, counters fired and the triggered logic configuration for each event.

In the course of the experiment we took approximately 750,000 pictures at 20 equally spaced energies between 1.1 and 2.0 GeV/c with tagging to invariant mass bins of ≈ 2.5 MeV.

Each picture was scanned and was required to have a good beam signature, converted gamma rays in the chambers and no antineutron star. Events meeting these criteria were then measured - three points on the beam line, conversion and direction point on each gamma, all in two views. Using the known positions of a set of fiducial lights on the chambers each point is reconstructed in space. A line is fit to the three beam points and an interaction point for the event is fit to the beam and directional information of all gammas.

Information on the measurement errors comes from the redundant measurement of the coordinate perpendicular to the gaps - which indicates a rms error of 5 mm - and from projections of the beam tracks into the downstream chamber for straight through tracks, which also gives

uncertainties of $\pm$ 5 mm. The interaction point is determined to $\pm$ 2 cm and is one of the larger sources of angular uncertainty.

It is a kinematical property of massive particles decaying into gamma ray pairs that the distribution of the opening angle, $\theta$, between the gammas is characterized by a sharp minimum angle with most of the events piling up near this minimum[1]. This minimum is a function only of the velocity, $\beta$, of the decaying particle, which in the center of mass of a two body event is unique. We have $\cos \frac{\theta_{min}}{2} = \beta$. At 1.752 GeV/c, $\theta_{min}$ for $\pi^\circ$ from $\bar{p}p \to \pi^\circ\pi^\circ$ is 13°; for $\bar{p}p \to \pi^\circ\eta^\circ$, $\theta_{min}$ is 13.8° for the $\pi^\circ$ and 52.2° for $\eta^\circ$.

Because of the efficiency of our system for detecting gamma rays, more than 95% of $\pi^\circ\pi^\circ$ and $\pi^\circ\eta^\circ$ events in which the $\pi^\circ$ and $\eta^\circ$ decay via two gamma are detected as either four gamma or three gamma events. Figures 3 and 4 show all pairs of center of mass opening angles for all three or four gamma events. Prominent in both are the $\pi^\circ$ peaks. To find the two body events we display on a scatter plot the smallest opening angle for each event versus the remaining opening angle (Fig. 5). The accumulation at the minimum opening angle for both pairs at the $\pi^\circ$ angle is apparent. There is also a clear accumulation at the $\eta^\circ$ angle.

We have one more kinematic variable in a two body process, namely the angle between directions of the decaying particles. In the center of mass these directions should have a relative angle of 180°. Using the bisector of the pairs as an approximation and making a cut at 15° on the angle between one bisector and the reflection of

the other, one sees a dramatic enhancement of signal to noise (Fig. 6). In practice one can do better by treating the sample as though they were all $\pi^\circ\pi^\circ$ or $\pi^\circ\eta^\circ$ events. Under these hypotheses one can calculate for each pair of gammas from an assumed $\pi^\circ$ or $\eta^\circ$ the two possible directions for the $\pi^\circ$ or $\eta^\circ$. There are two possible solutions, symmetrically disposed on either side of the bisector, since we do not distinguish which gamma has the higher energy. For each event we select the two directions which are closest to 180° apart. In Figure 7 we show the reflected relative angle distribution for pairs passing cuts on the opening angle (smaller $\theta < 21°$, larger $\theta < 30°$). Also shown is the relative angle distribution for three gamma events, which we determine between the solution of the pair (with $\theta < 30°$) closest to 180° to the odd gamma. For the three gamma events we display the smallest opening angle versus the relative angle to show the accumulation at the $\pi^\circ\pi^\circ$ region (Fig. 8).

There is some contamination of background in both of these samples, which arise from systems of higher multiplicity, e.g., three $\pi^\circ$ or four $\pi^\circ$, and which are not detected in their entirety in the equipment. To estimate this background we generate events by eliminating short gammas from observed events having five or more gammas. These are most probably the gammas that would be lost due to detection inefficiencies and would give rise to lower multiplicity events. Treating those events that become four gammas under this operation as a background sample we normalize to the region outside the $\pi^\circ\pi^\circ$ and $\pi^\circ\eta^\circ$ regions on the scatter plot of the data events and perform a subtraction. For the three gamma events we use the opening angle versus the relative angle scatter plot to ascertain the background.

For the three gamma $\pi^\circ\pi^\circ$ events there is an additional background from the $\pi^\circ\eta^\circ$ events where one of the $\eta^\circ$ gammas is missed. In fact ≃ one half of the number that appear in the $\pi^\circ\eta^\circ$ region would fall into $\pi^\circ\pi^\circ$ region. This is calculated using a Monte Carlo program. The final raw angular distributions for $\pi^\circ\pi^\circ$ and $\pi^\circ\eta^\circ$ events passing the cuts are shown in Figures 9, 10, and 11. We use as an estimate of the polar angle for each event the direction obtained by appropriately averaging the two space vectors representing the $\pi^\circ\pi^\circ$ or $\pi^\circ\eta^\circ$ for each event.

In order to correct these distributions for triggering biases and efficiency, geometric detection inefficiencies and experimental resolution, we use a Monte Carlo simulation program. To check the results of this program we have used several calibrations. First, we are able to predict correctly the number of gamma rays converting in our lead scintillator hodoscope, for a given number of gamma rays incident upon the detector, by determining the number of gammas as a function of distance into the chamber and extrapolating back to the beginning to find the excess over an exponential rise. Second, we can predict the number of counters fired and compare with the data, since this is encoded on each picture. Third, we are able to predict the number of events which are visible as four gamma or three gamma events as a function only of an effective low energy cut-off on visible gammas in the chambers, which we can adjust to fit the data. Fourth, the Monte Carlo events spread with the experimental measurement errors agrees with the data in opening angle distribution, relative angle distribution, etc. (See Figure 7.)

To reconstruct angular distributions from the raw data we need to generate with the Monte Carlo a matrix which gives the probability for detecting an event in $dx'$ at $x' = \cos\theta'$ if it actually occurred in $dx$ at $x = \cos\theta$.

(5)

To do this we define a density M(x,x') such that the observed distribution n'(x') can be gotten from the true parent distribution n(x) by

$$n'(x')dx' = dx' \int_{-1}^{+1} dx M(x,x') n(x)$$

with M(x,x')dx' = probability that an event produced at x is detected in dx' at x', and $\int_{-1}^{+1} M(x,x')dx'$ = total probability, with our equipment, cuts, etc. of detecting an event produced at x. Expanding n(x) in Legendre polynomials:

$$n(x) = \sum_{\ell=0}^{L_{max}} a_\ell P_\ell(x)$$

and

$$n_i = \int_{\substack{i\text{-th} \\ \text{bin}}} n'(x')dx' = \sum_{\ell=0}^{L_{max}} a_\ell \int_{\substack{i\text{-th} \\ \text{bin}}} dx' \int M(x,x') P_\ell(x) n(x) dx = \sum_{\ell=0}^{L_{max}} a_\ell M_{\ell i}$$

where $n_i$ is the number of events in the ith bin of the observed variable x'. We evaluate the $M_{\ell i}$ by Monte Carlo techniques. The problem of determining the parent distribution, i.e., the $a_\ell$, is just a linear fitting problem. The final check on the veracity of the Monte Carlo is done by generating separate $M_{\ell i}$ for the three gamma sample, the four gamma sample, and the sum of both (which is almost independent of the detection efficiency) and fitting each sample separately. All of these should predict the same parent distribution both in shape and in number. The results of these fits are given in Figure 12 for the $\pi^0\pi^0$. It is encouraging that the fitted distributions and the normalization come out so similar to each other in the three gamma and four gamma cases, especially since the raw samples are so dissimilar (Figures 9, 10). In Figure 13

we show the results of the fit to the $\pi^\circ\eta^\circ$ sample. Because of the symmetries of the two processes the differential cross section of both $\bar{p}p \to \pi^\circ\pi^\circ$ and $\bar{p}p \to \pi^\circ\eta^\circ$ are restricted to even Legendre polynomial expansions. We fit for successively increasing values of $L_{max}$ and stopped adding terms when the probability for the fit reached reasonable values and stabilized. In Figure 14 we show the situation for the $\pi^\circ\pi^\circ$ case. We accepted $L_{max} = 8$ and rejected $L_{max} = 10$ because the $a_{10}$ that was required was consistent with 0.

We can convert these numbers of parent events to true differential cross sections by combining them with electronic triggering rate data acquired during the experiment and by making suitable corrections for various losses. This calculation is outlined in Table I.

The integrated cross section for $\bar{p}p \to \pi^\circ\pi^\circ$ at 1.752 GeV/c is 12.85 $\pm$ 1.2 μb, where the error is statistical. There is an additional overall uncertainty in the normalization, which we estimate at this time to be ≈ 10%.

In Table II we list the properly normalized coefficients $a_\ell$ in the expansion

$$\frac{d\sigma}{d\Omega} = \sum_{\ell=0}^{L_{max}} a_\ell P_\ell(x)$$

Also listed are the coefficients in a similar expansion for the process $\bar{p}p \to \pi^+\pi^-$ from the data of Eisenhandler et al.[2]. We have averaged the fits of these authors to their data at 1.70 and 1.80 GeV/c to compare with our data at 1.752 GeV/c.

If we represent the two π annihilation process by two I spin amplitudes, $M_0$ and $M_1$,

then $M_{+-} = M_0 + M_1$

and $M_{00} = M_0$

then $$\frac{d\sigma_{+-}}{d\Omega} = |M_0|^2 + |M_1|^2 + 2\mathrm{Re}M_0M_1^*$$

$$\frac{d\sigma_{00}}{d\Omega} = |M_0|^2$$

Initial spin state indices and averages have been suppressed in the above. Since the dipion state must be symmetric, including the I spin variable, the amplitudes $M_1$ and $M_0$ must be composed of odd and even spherical harmonics respectively. This implies that $|M_1|^2$ and $|M_0|^2$ have purely even expansions in Legendre polynomials and only the interference term gives rise to the odd terms in the expansion of the cross section.

Since the $\pi^\circ\pi^\circ$ measurement determines $|M_0|^2$ separately, we can subtract it from the $\pi^+\pi^-$ expansion and the remaining odd and even terms are separately $M_1{}^2$ and $2\mathrm{Re}M_0M_1^*$. This separation is shown in the last two columns of Table II and the separate angular functions are displayed in Figure 15.

The most outstanding feature of the Legendre polynomial fits to the $\pi^\circ\pi^\circ$ data is the large $a_8$ coefficient. The other coefficients, aside from $a_0$, which basically determines the total cross section for the reaction, are all small. Due to the fact that the two pi annihilation takes place from the triplet $\bar{p}p$ states only, the general form of the amplitude contains only incoherent sums of spherical harmonics with m = 0 and $\pm 1$[3]. This fact, coupled to the obviously related observation that the differential cross section has a very strong dip-peak structure with almost hard zeros tempts one to try to interpret the data in terms of the simplest amplitude possible.

Obviously such a procedure is subject to many ambiguities and a more rigorous analysis will have to await the reduction of the remainder of our data over the whole energy range. The results of an incomplete search for various combinations of functions which could fit the data are given in Table III. In fact we found that we had very little freedom to chose various combinations of functions and we reproduce our best almost unique solutions. The following comments are in order: $|M_0|^2$ is quite adequately describable as $|aY_2^\circ + bY_4^\circ|^2$ with a and b very close to 180° out of phase. It will be interesting to see whether this analysis holds up at neighboring energies and whether either a or b varies rapidly with energy as would happen if there were an I = 0, J = 2 or 4 resonance in this region. We note in passing that the energy of this experiment is close to the center of the broad maximum in the $\bar{p}p$ and $\bar{p}n$ total cross sections[4] that has been suggested to be due to both an I =0 and I = 1 resonance in this energy region. The momentum bite covered by this experiment was ≈ 85 MeV/c and each event was tagged to ± 3.5 MeV/c incident momentum. We searched for possible variation in the angular distribution across this region (≈ 30 MeV in mass) and within the limited statistics available we see no strong variation in the angular distribution. (See Figure 16.) In this connection, the reaction $\bar{p}p \to \pi^\circ\eta^\circ$ is pure $I^G = 1^-$ and seems to have a very different angular momentum composition than the I = 1 part of $\bar{p}p \to \pi^+\pi^-$ (which is $I^G = 1^+$). (See Figures 13 and 15.)

The $|M_1|^2$ angular distributions turned out to yield somewhat less satisfactory solutions after a similar search. While we get very good reproductions of the angular distributions with the parameters indicated in Table II, the coefficients are not consistent with those that would arise from a proper amplitude squared. There is considerable sensitivity to the relative normalization

of the two experimental input samples, particularly with regard to the magnitude of the coefficients of the $Y_3^1 Y_5^1$ and $Y_5^1 Y_1^1$ terms.

What is clearly needed in order to search for possible resonances in these systems is to complete the set of angular distributions of $\bar{p}p \to \pi^\circ\pi^\circ$ to enable us to perform the separation into I = 1 and I = 0 cross sections in combination with the data of Reference 2. We can then attempt an energy dependent parameterization of amplitudes including varying background terms.

In conclusion, the first angular distributions we have obtained in these neutral two body processes show great promise for aiding in the understanding of the rich structure in the $\bar{p}p$ annihilations. Over the next year we will have substantially more data and will attempt a more thorough analysis.

We gratefully acknowledge the expert technical assistance of Mr. T. Lyons and his group at Brookhaven and Mr. A. Distante and his group at Bari and the excellent work of our various scanning staffs. We wish to thank Messrs. W. Aitkenhead, J. Butler, and S. Redner for their assistance during the construction, running and preliminary data analysis.

## References


1. B. Rossi, High Energy Particles (Prentice Hall, Inc., Englewood Cliffs, New jersey, 1962), p. 198.

2. E. Eisenhandler et al., Phys. Lett. B47, 531 (1973), and A. Astbury, private communication.

3. H. Nicholson et al., Phys. Rev. D7, 2585 (for a general expression for $d\sigma/d\Omega$ for 2 $\pi$ annihilation).(1973)

4. R.J. Abrams et al., Phys. Rev. D1, 1917 (1970).

5. F. Bulos et al., Phys. Rev. 187, 1827 (1969).

# Tables

Table I

1.752 GeV/c

$$\sigma_{\pi^\circ\pi^\circ} = \frac{N_{\text{MCarlo Parents}}}{N_{\text{Good Trigger}}} \times (R_{\text{full}} - R_{\text{empty}}) \times F_{\text{corr}} \times \frac{1}{N_\circ \rho_{H_2} L}$$

$N_{\text{MCarlo Parents}} = 520.6$

$N_{\text{Good Trigger}} = 11206$

$R_{\text{full}} = 1.05 \times 10^{-4} \text{ev}/\bar{p}$

$R_f - R_e = 9.66 \times 10^{-5} \text{ev}/\bar{p}$

$R_{\text{empty}} = 8.4 \times 10^{-6} \text{ev}/\bar{p}$

$F_{\text{corr}} = (1.06)_{\gamma \text{ conversion}} (1.019)_{\bar{p}\text{atten}} (1.024)_{\text{Dalitz}} (1.0055)_{\text{Shrink}}$

$= 1.112$

$\rho_{H_2} = 0.0708$ g/cc

$L = 9.2$ cm

$$\sigma_{\pi^\circ\pi^\circ} = 12.85 \pm 1.2 \ \mu\text{b}$$

$$M^{+-} = M^{\circ} + M^{1}$$

$$M^{\circ\circ} = M^{\circ}$$

$$M^{\circ}(\theta) = M^{\circ}(\pi - \theta) \qquad M^{1}(\theta) = -M^{1}(\pi - \theta)$$

$$\frac{d\sigma^{+-}}{d\Omega}(\theta) = |M^{\circ}|^2 + |M^{1}|^2 + 2\,\mathrm{Re}\,M^{\circ}M^{1*}$$

$$= \sum_{\ell\ \mathrm{even}} a_\ell^{\circ} P_\ell + \sum_{\ell\ \mathrm{even}} a_\ell^{1} P_\ell + \sum_{\ell\ \mathrm{odd}} a_\ell^{01} P_\ell$$

$$\frac{d\sigma^{\circ\circ}}{d\Omega}(\theta) = |M^{\circ}|^2 = \sum_{\ell\ \mathrm{even}} a_\ell^{\circ} P_\ell$$

$$\frac{d\sigma^{+-}}{d\Omega} - \frac{d\sigma^{\circ\circ}}{d\Omega} = |M^{1}|^2 + 2\,\mathrm{Re}\,M^{\circ}M^{1*}$$

$$= \sum_{\ell\ \mathrm{even}} a_\ell^{1} P_\ell + \sum_{\ell\ \mathrm{odd}} a_\ell^{01} P_\ell$$

$$\sigma_{I=1}^{\mathrm{tot}} = \int_{4\pi} \left(\frac{d\sigma^{+-}}{d\Omega} - \frac{d\sigma^{\circ\circ}}{d\Omega}\right) d\Omega = \sigma^{+-} - 2\sigma^{\circ\circ}$$

$$\sigma_{I=0}^{\mathrm{tot}} = 3\sigma^{\circ\circ}$$

Table II

1.75 BeV/c Legendre Coefficients

| $\ell$ | $a_\ell^{\circ}$ | $a_\ell^{\circ} + a_\ell^{1} + a_\ell^{01}$ | $a_\ell^{1}$ | $a_\ell^{01}$ $\mu$b/sr |
|---|---|---|---|---|
| 0 | 2.05 ± .19 | 7.85 ± .17 | 5.8 ± .23 | |
| 1 | | .67 ± .34 | | .67 ± .34 |
| 2 | -.15 ± .43 | -.13 ± .44 | .2 ± .55 | |
| 3 | | 2.03 ± .52 | | 2.03 ± .52 |
| 4 | .78 ± .65 | 0.1 ± .66 | -.68 ± .83 | |
| 5 | | 5.90 ± .65 | | 5.90 ± .65 |
| 6 | -1.46 ± .73 | 5.57 ± .69 | 7.03 ± .89 | |
| 7 | | -.32 ± .73 | | -.32 ± .73 |
| 8 | 4.32 ± .89 | 12.8 ± .8 | 8.48 ± 1.06 | |
| 9 | | .44 ± .8 | | .44 ± .8 |
| 10 | | -2.46 ± .92 | -2.46 ± .92 | |

Table III

## Amplitude Analysis
(in μb/sr)

$$|M_0|^2 = (39.3\pm6)|Y_{40}|^2 - (59.6\pm7.7)|Y_{40}Y_{20}| + (18.3\pm7)|Y_{20}|^2$$

$$\underline{\text{Prob}(X^2) \simeq 65\%}$$

$$|M_1|^2 = (22.17\pm8)|Y_{51}|^2 + (64.3\pm8.9)|Y_{31}|^2 + (80.3\pm7.9)|Y_{30}|^2 - (130.6\pm10.7)|Y_{51}Y_{31}| + (117.4\pm28.7)|Y_{51}Y_{11}|$$

$$\underline{\text{Prob}(X^2) \simeq 35\%}$$

$$2\text{Re}|M_1M_0^*| = (53.9\pm16)|Y_{40}Y_{10}| - (38.7\pm12)|Y_{20}Y_{10}| + (31.0\pm7.5)|Y_{20}Y_{30}| - (3.3\pm7.5)|Y_{40}Y_{30}|$$

$$\underline{\text{Prob}(X^2) \simeq 75\%}$$

# List of Illustrations

Figure 1

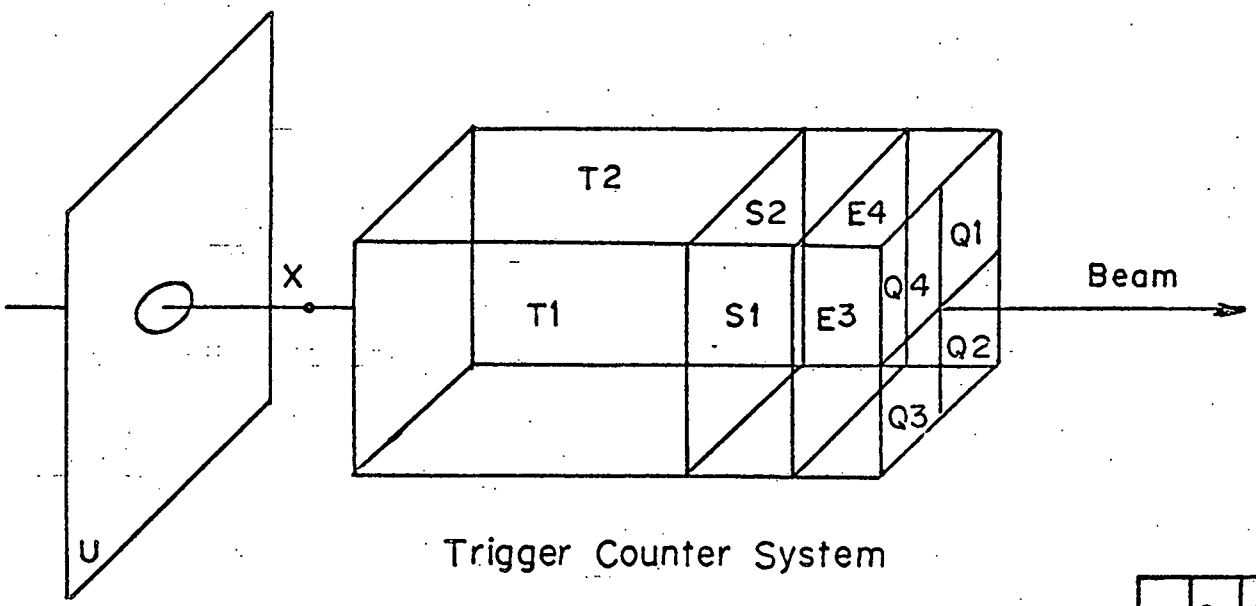


Trigger Counter System

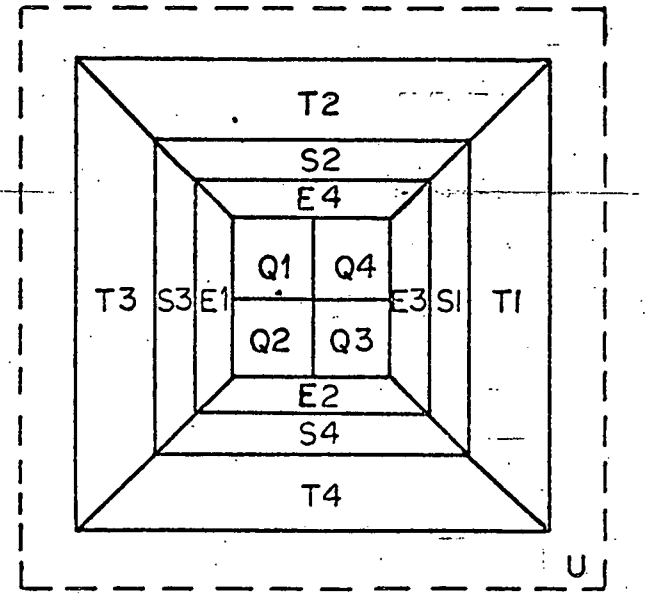


View looking downstream from X

| | S1 T1 | S2 T2 | S3 T3 | S4 T4 | S1 | S2 | Q | E |
|---|---|---|---|---|---|---|---|---|
| Q1 | X | | | X | | | | |
| Q2 | X | X | | | | | | |
| Q3 | | X | X | | | | | |
| Q4 | | | X | X | | | | |
| E1 | X | | | | | | | |
| E2 | | X | | | | | | |
| E3 | | | X | | | | | |
| E4 | | | | X | | | | |
| S3 | | | | | X | | | |
| S4 | | | | | | X | | |
| U | | | | | | | X | X |

logic pair

Trigger Counters

Figure 2

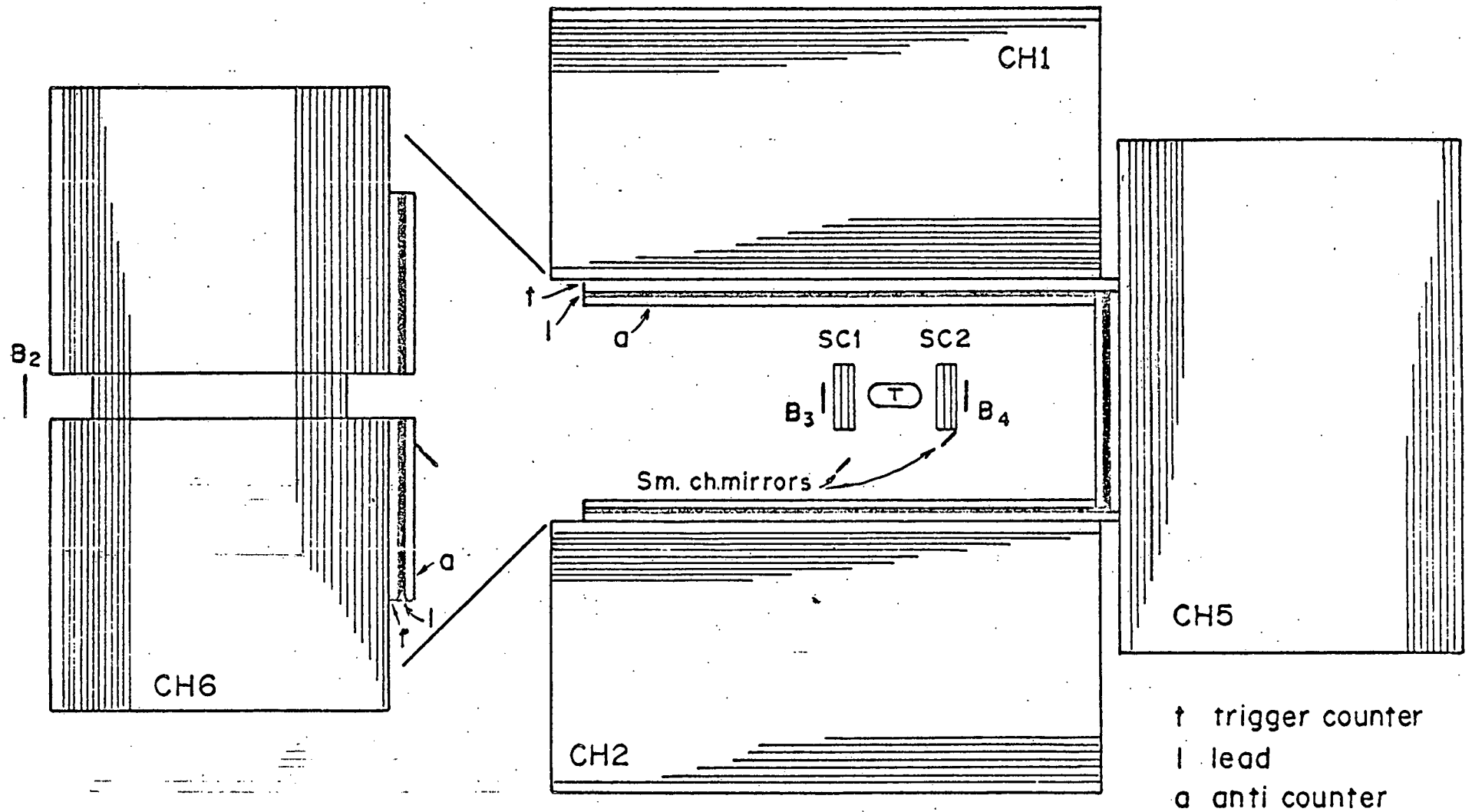
CH1
CH5
CH6
CH2
B2
t
l
a
SC1
SC2
B3
T
B4
Sm. ch.mirrors
t trigger counter
l lead
a anti counter

Figure 3

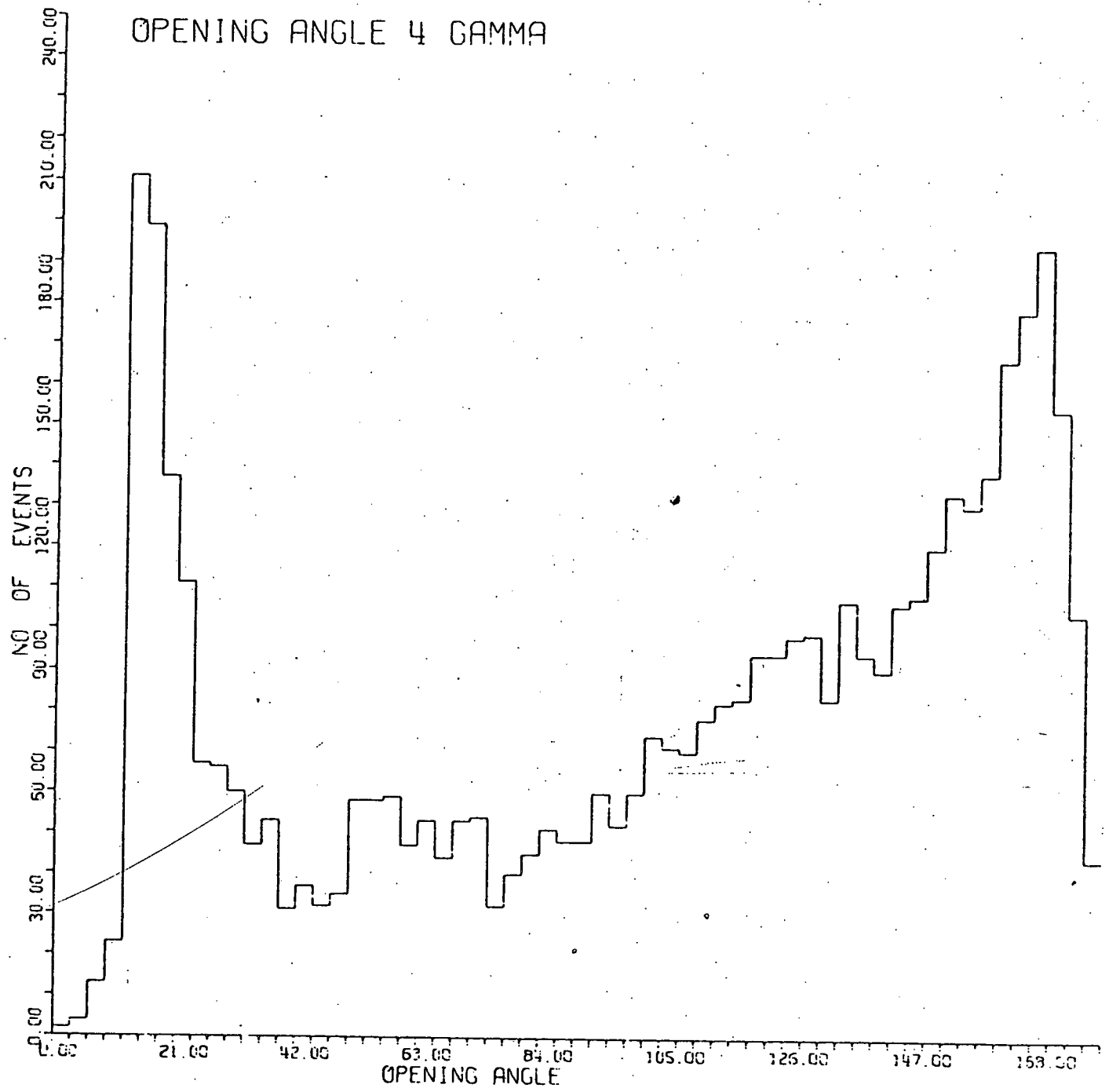
OPENING ANGLE 4 GAMMA
NO OF EVENTS
0.00
30.00
60.00
90.00
120.00
150.00
180.00
210.00
240.00
0.00
21.00
42.00
63.00
84.00
105.00
126.00
147.00
168.00
OPENING ANGLE

Figure 4

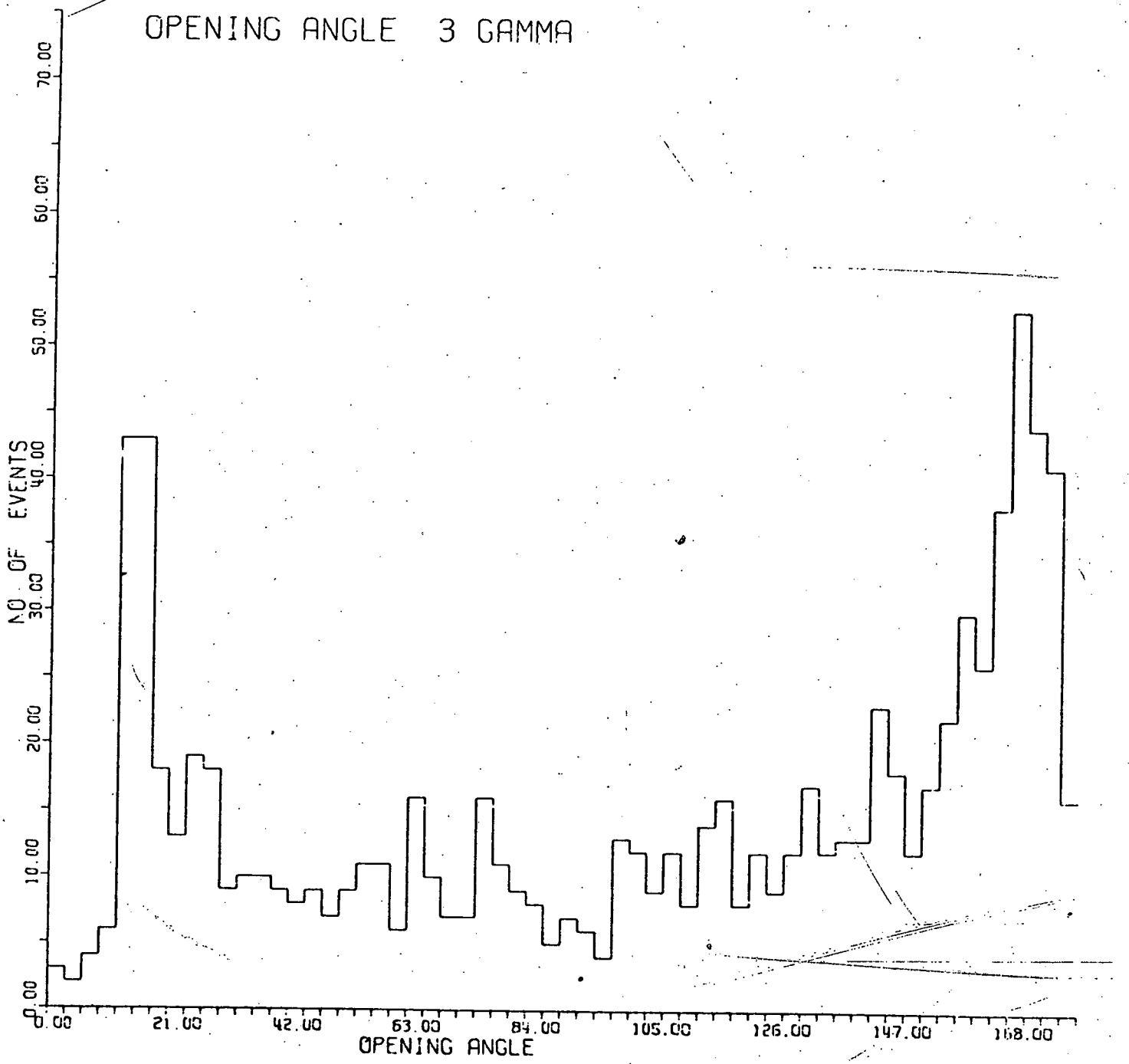
OPENING ANGLE 3 GAMMA
NO. OF EVENTS
0.00
10.00
20.00
30.00
40.00
50.00
60.00
70.00
0.00
21.00
42.00
63.00
84.00
105.00
126.00
147.00
168.00
OPENING ANGLE

Figure 5

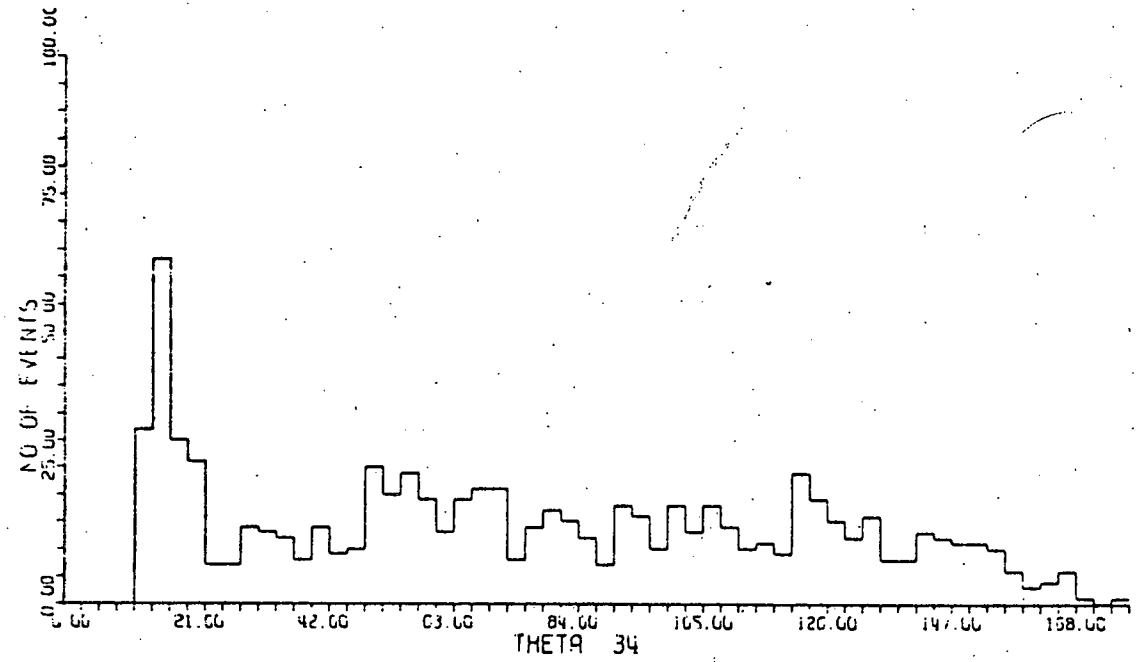
NO OF EVENTS
THETA 34

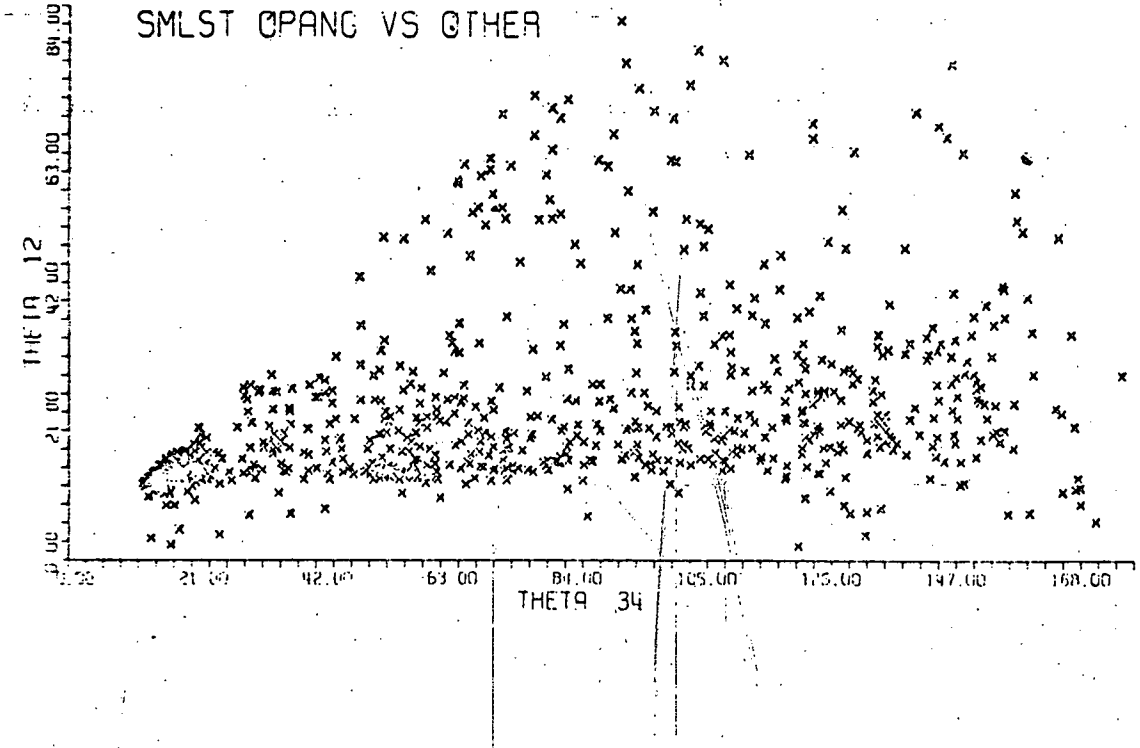
SMLST OPANG VS OTHER
THETA 12
THETA 34

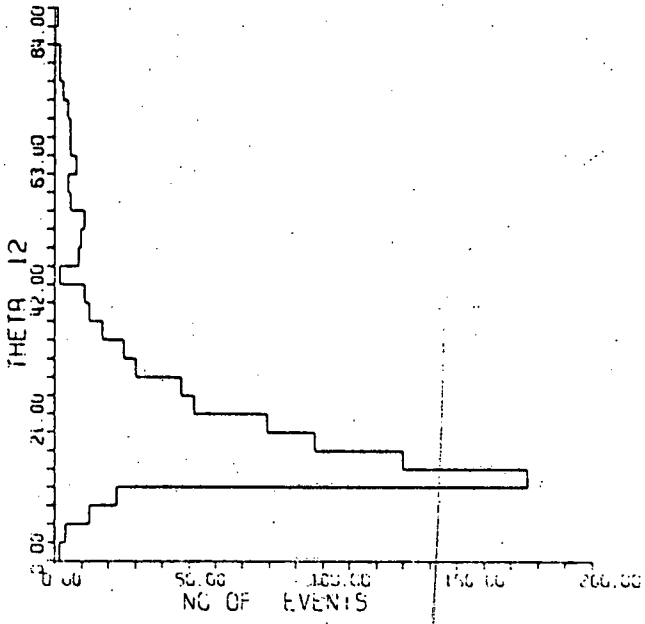
THETA 12
NO OF EVENTS

Figure 6

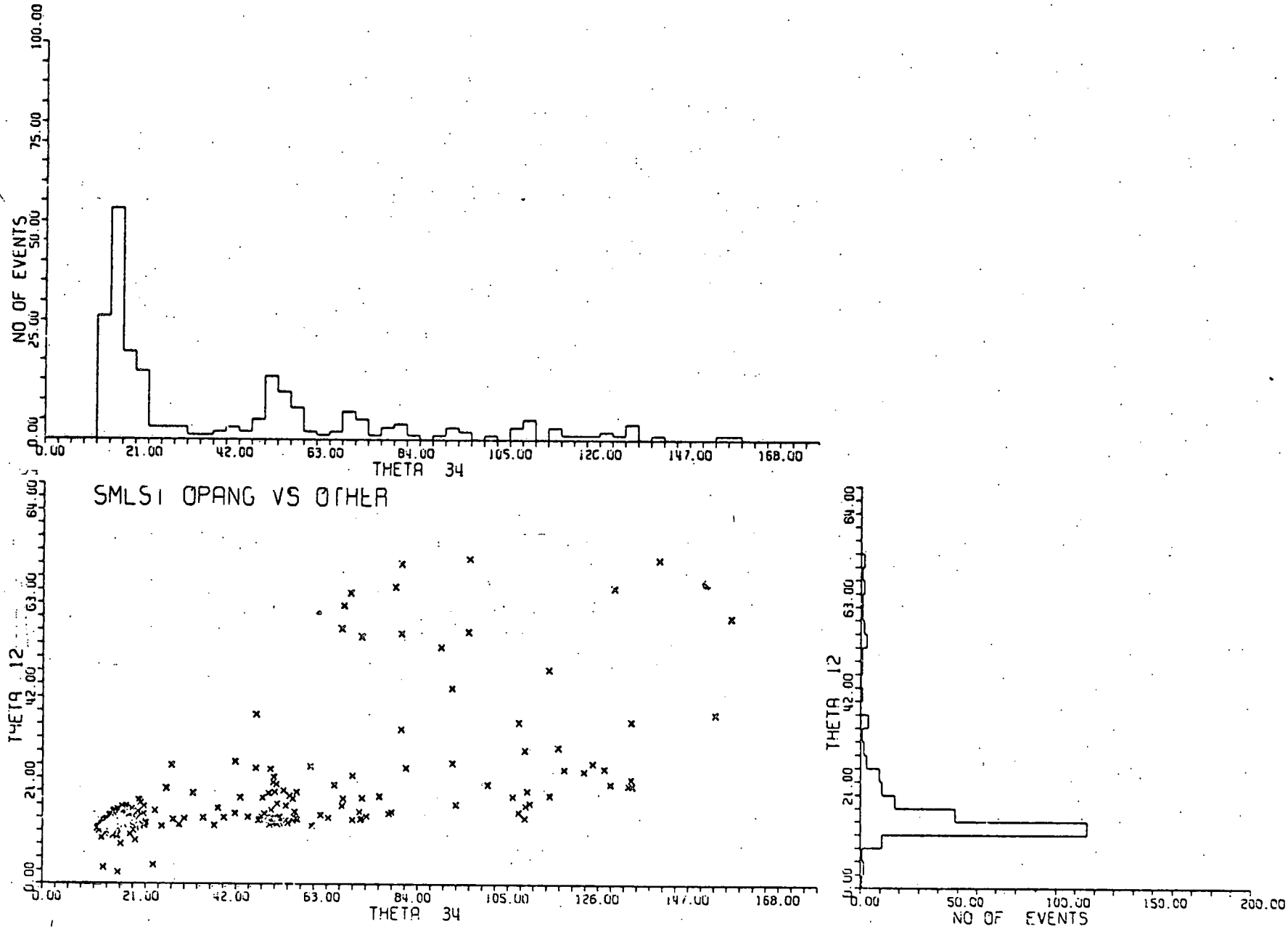
NO OF EVENTS
0.00
25.00
50.00
75.00
100.00
0.00
21.00
42.00
63.00
84.00
105.00
126.00
147.00
168.00
THETA 34
SMLS1 OPANG VS OTHER
THETA 12
0.00
21.00
42.00
63.00
84.00
THETA 34
105.00
126.00
147.00
168.00
THETA 12
0.00
21.00
42.00
63.00
84.00
0.00
50.00
100.00
150.00
200.00
NO OF EVENTS

Figure 7

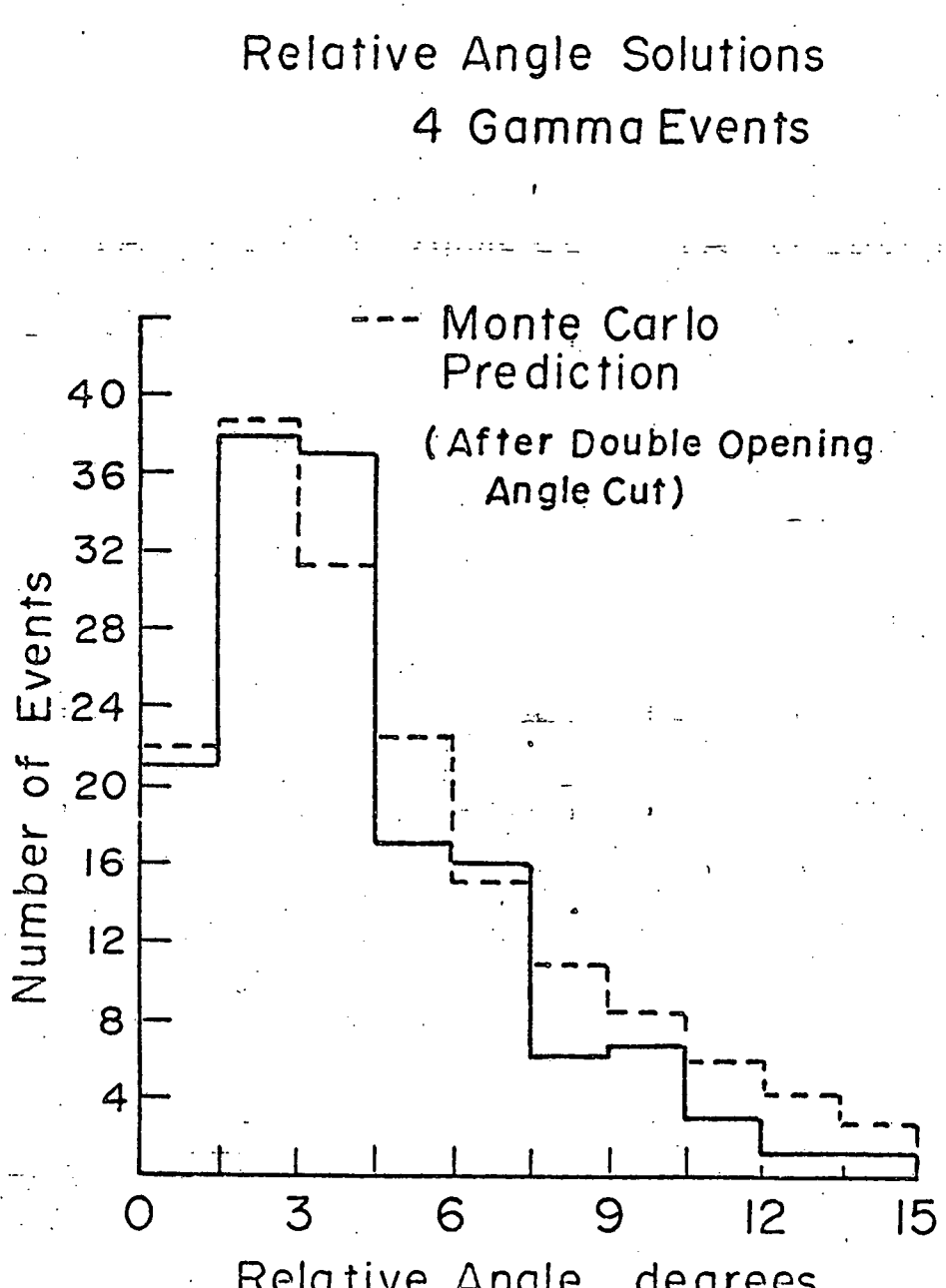
Relative Angle Solutions
4 Gamma Events
--- Monte Carlo Prediction
(After Double Opening Angle Cut)
Number of Events
40
36
32
28
24
20
16
12
8
4
0
3
6
9
12
15
Relative Angle , degrees

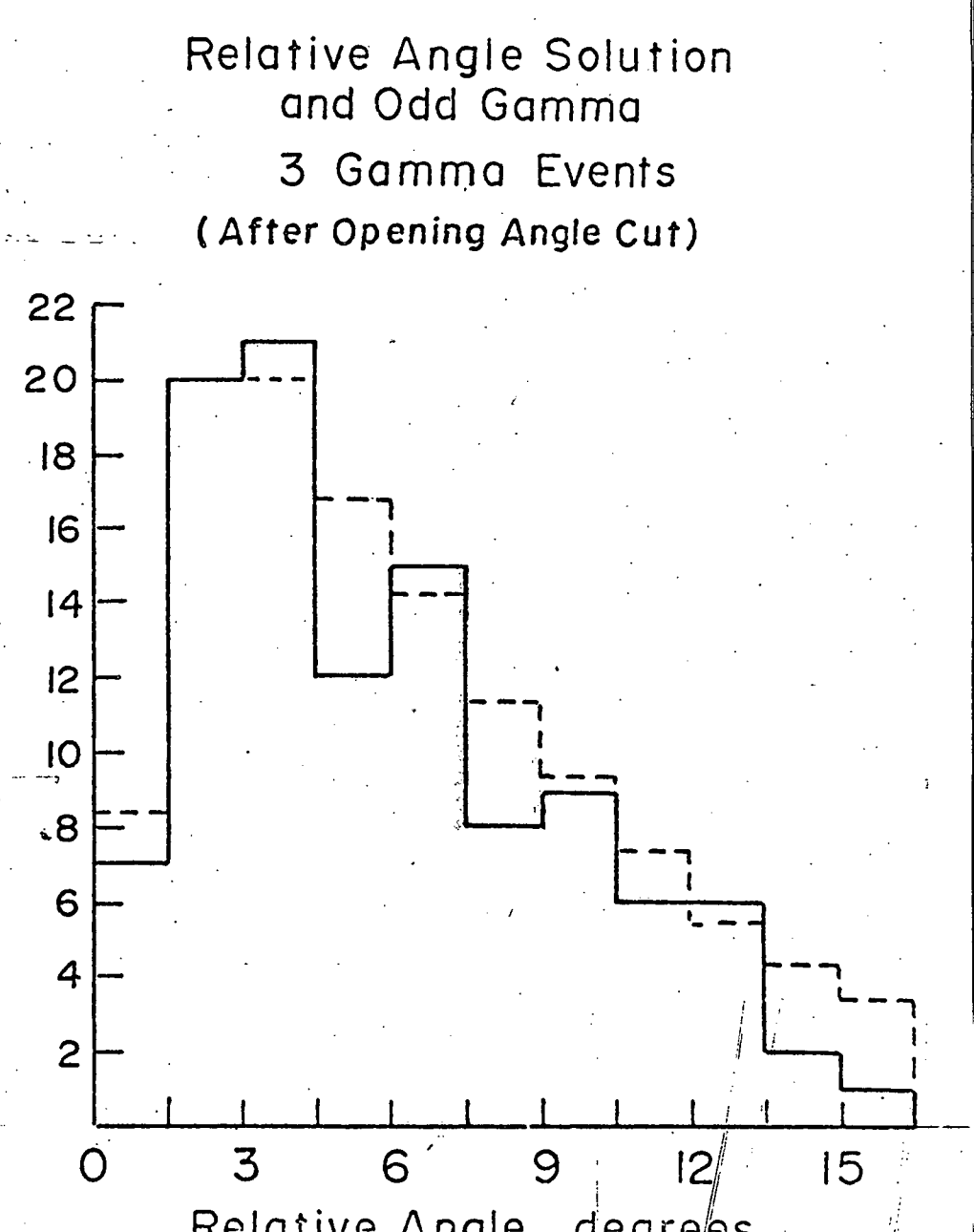
Relative Angle Solution and Odd Gamma
3 Gamma Events
(After Opening Angle Cut)
22
20
18
16
14
12
10
8
6
4
2
0
3
6
9
12
15
Relative Angle , degrees

Figure 8

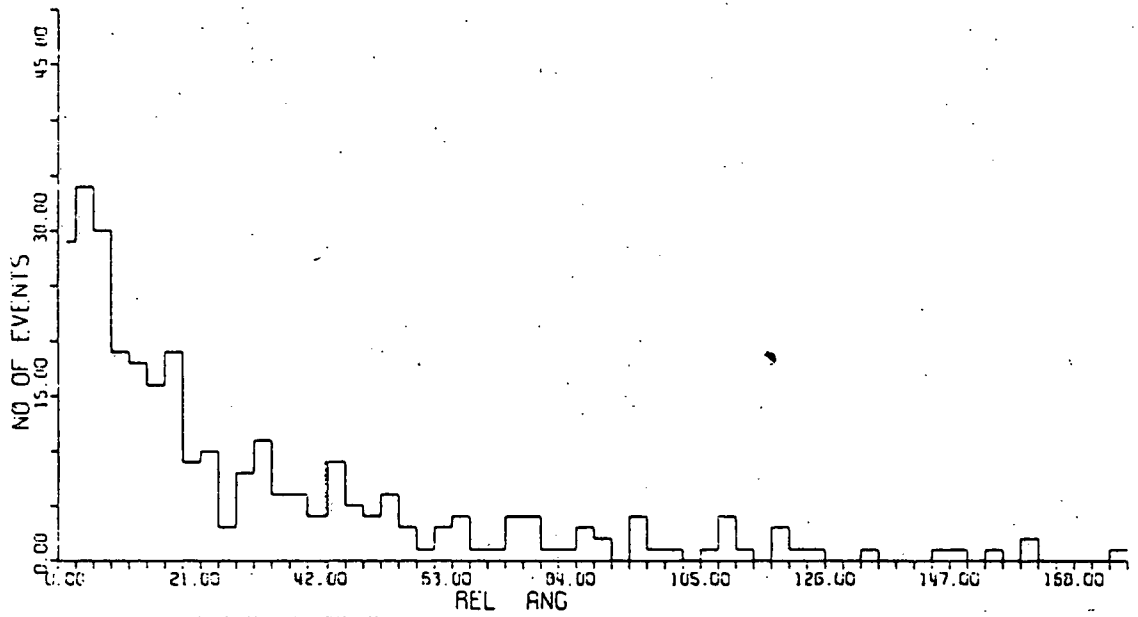
NO OF EVENTS
0.00
15.00
30.00
45.00
0.00
21.00
42.00
63.00
84.00
105.00
126.00
147.00
168.00
REL ANG

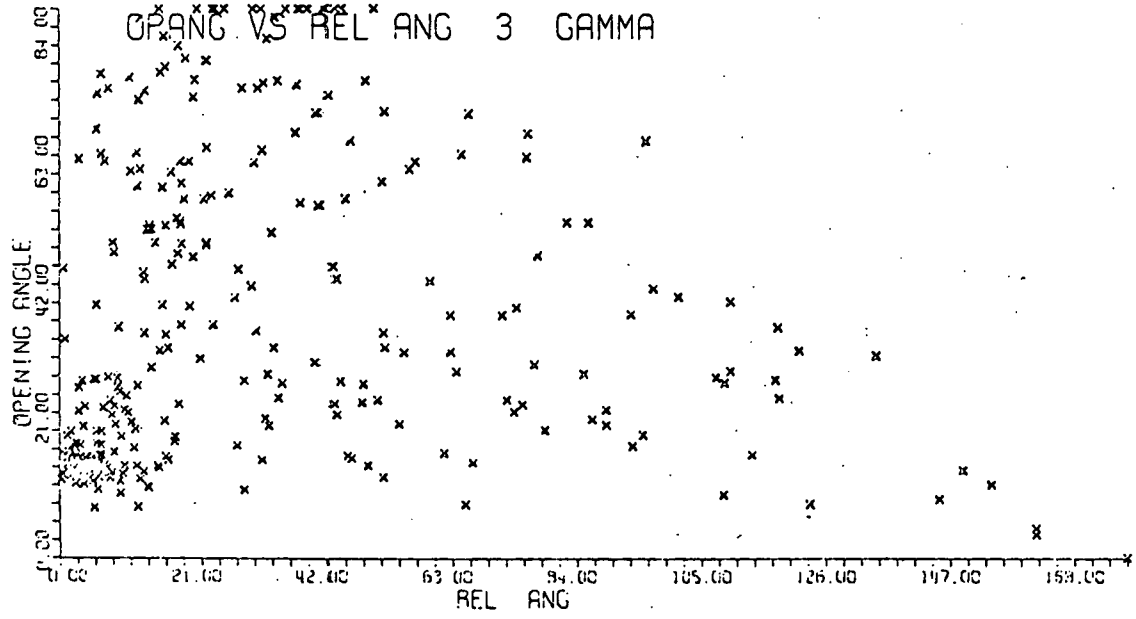
OPANG VS REL ANG 3 GAMMA
OPENING ANGLE
0.00
21.00
42.00
63.00
84.00
0.00
21.00
42.00
63.00
84.00
105.00
126.00
147.00
168.00
REL ANG

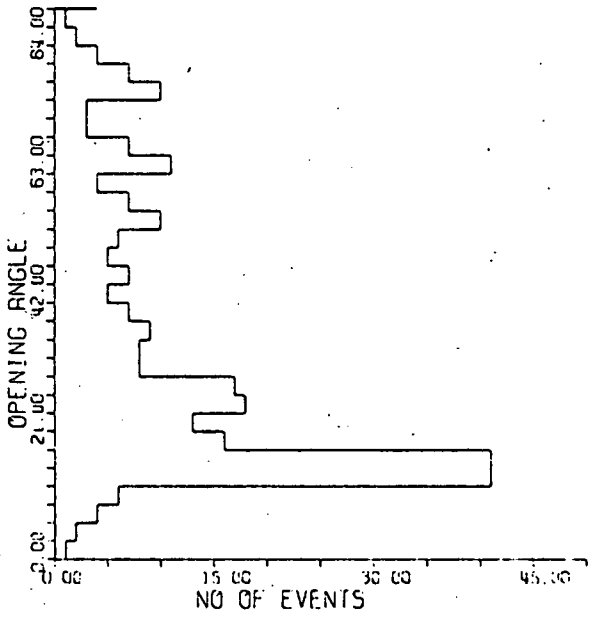
OPENING ANGLE
0.00
21.00
42.00
63.00
84.00
0.00
15.00
30.00
45.00
NO OF EVENTS

Figure 9

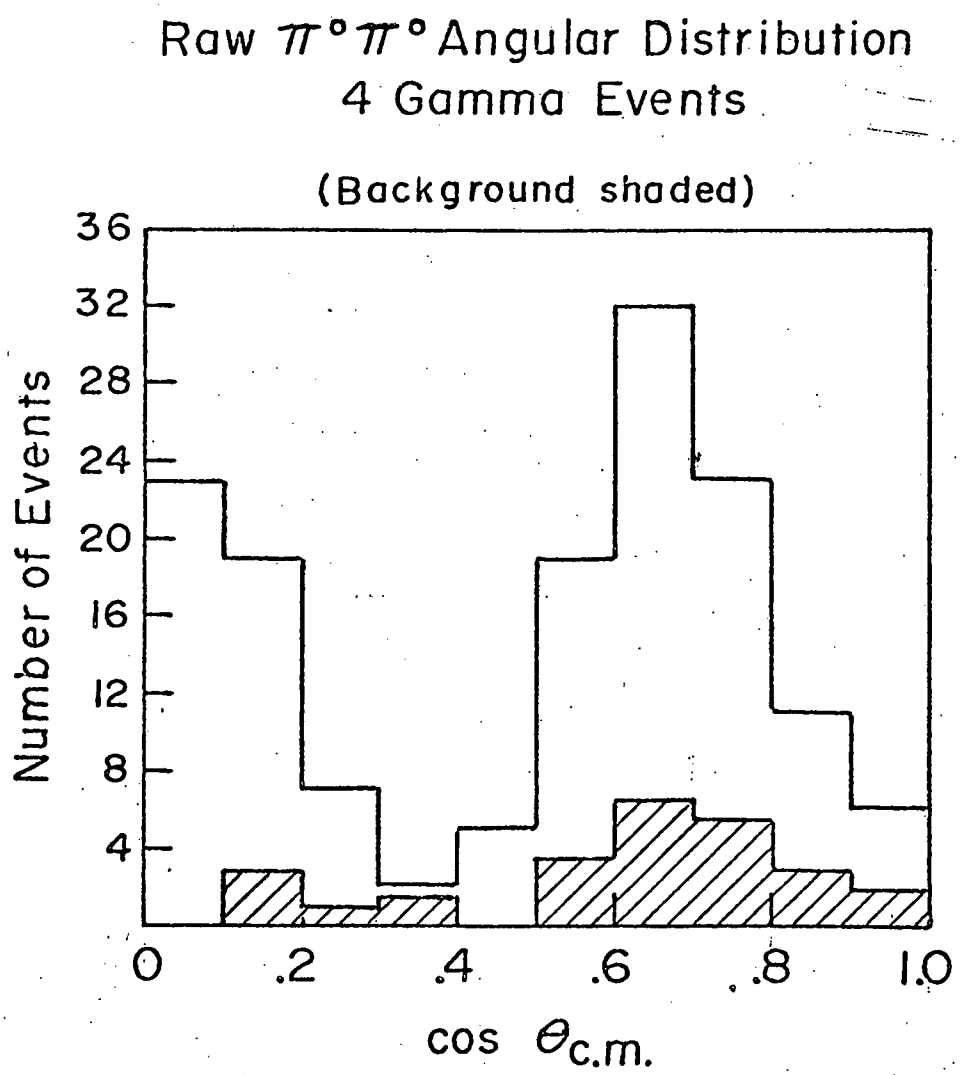
Raw $\pi^0\pi^0$ Angular Distribution
4 Gamma Events
(Background shaded)
Number of Events
36
32
28
24
20
16
12
8
4
0
.2
.4
.6
.8
1.0
cos $\theta_{c.m.}$

Figure 10

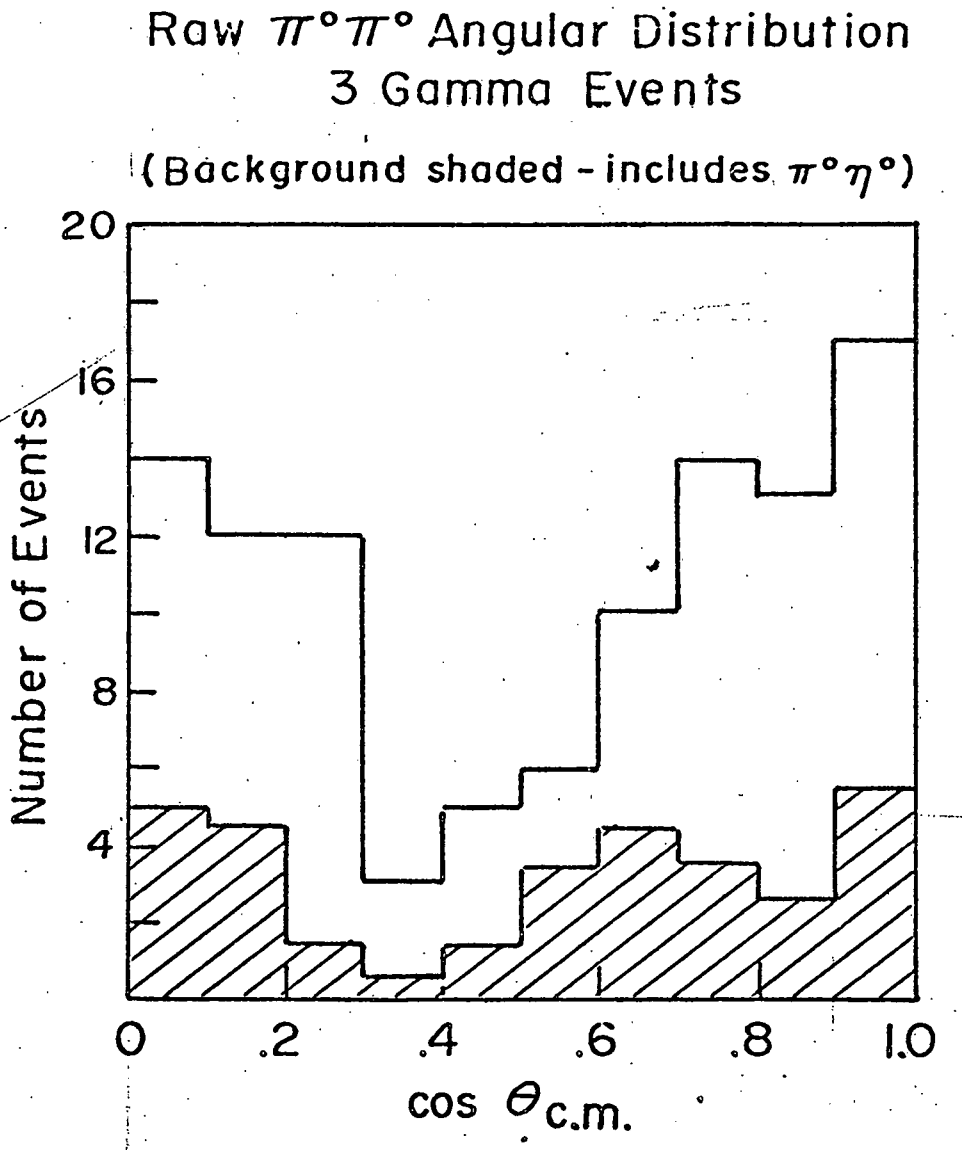
Raw $\pi^\circ\pi^\circ$ Angular Distribution
3 Gamma Events
(Background shaded - includes $\pi^\circ\eta^\circ$)
Number of Events
20
16
12
8
4
0
.2
.4
.6
.8
1.0
cos $\theta_{c.m.}$

Figure 11

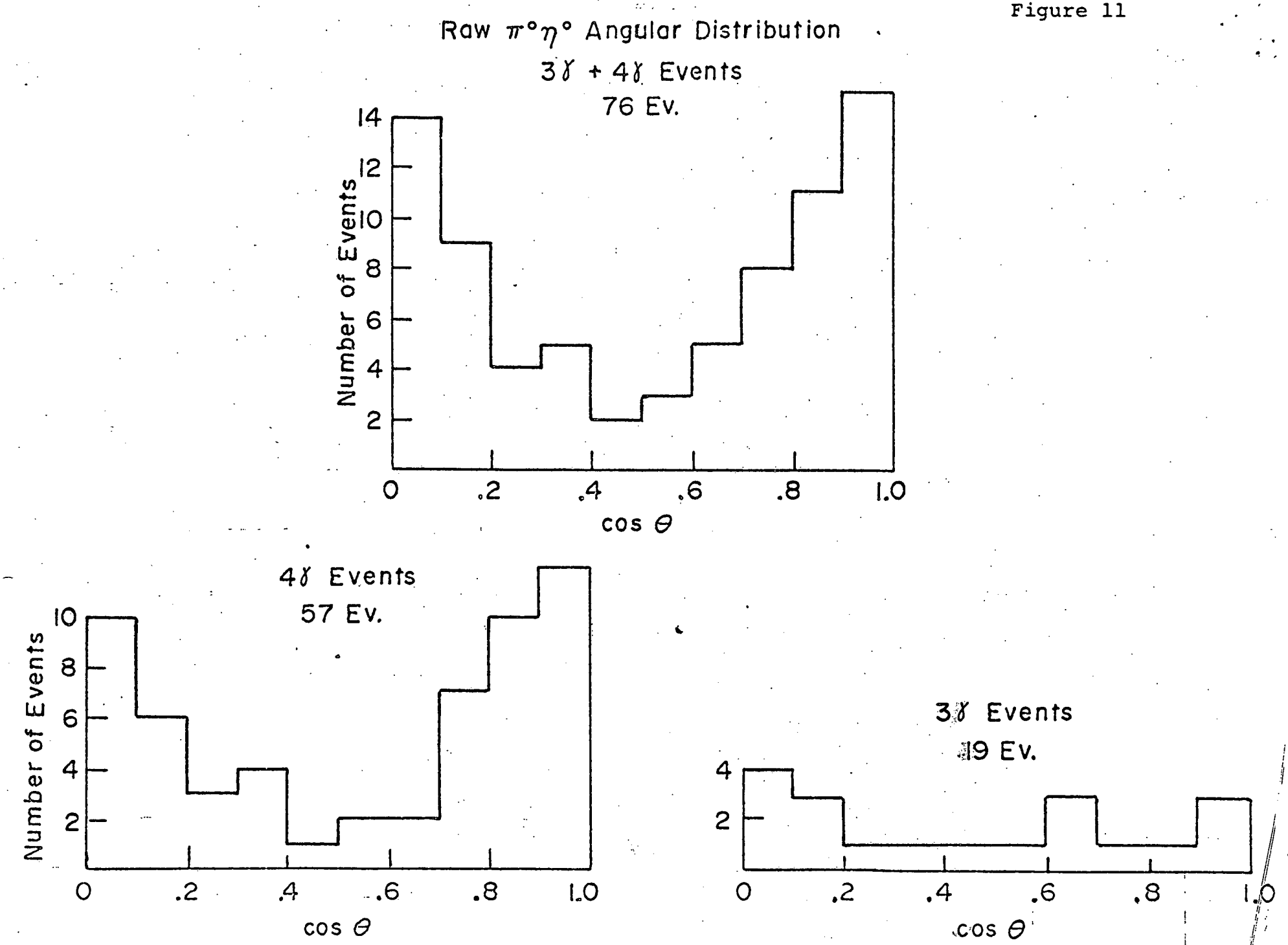
Raw $\pi^\circ\eta^\circ$ Angular Distribution
3γ + 4γ Events
76 Ev.
Number of Events
cos θ
4γ Events
57 Ev.
Number of Events
cos θ
3γ Events
19 Ev.
cos θ

Figure 12

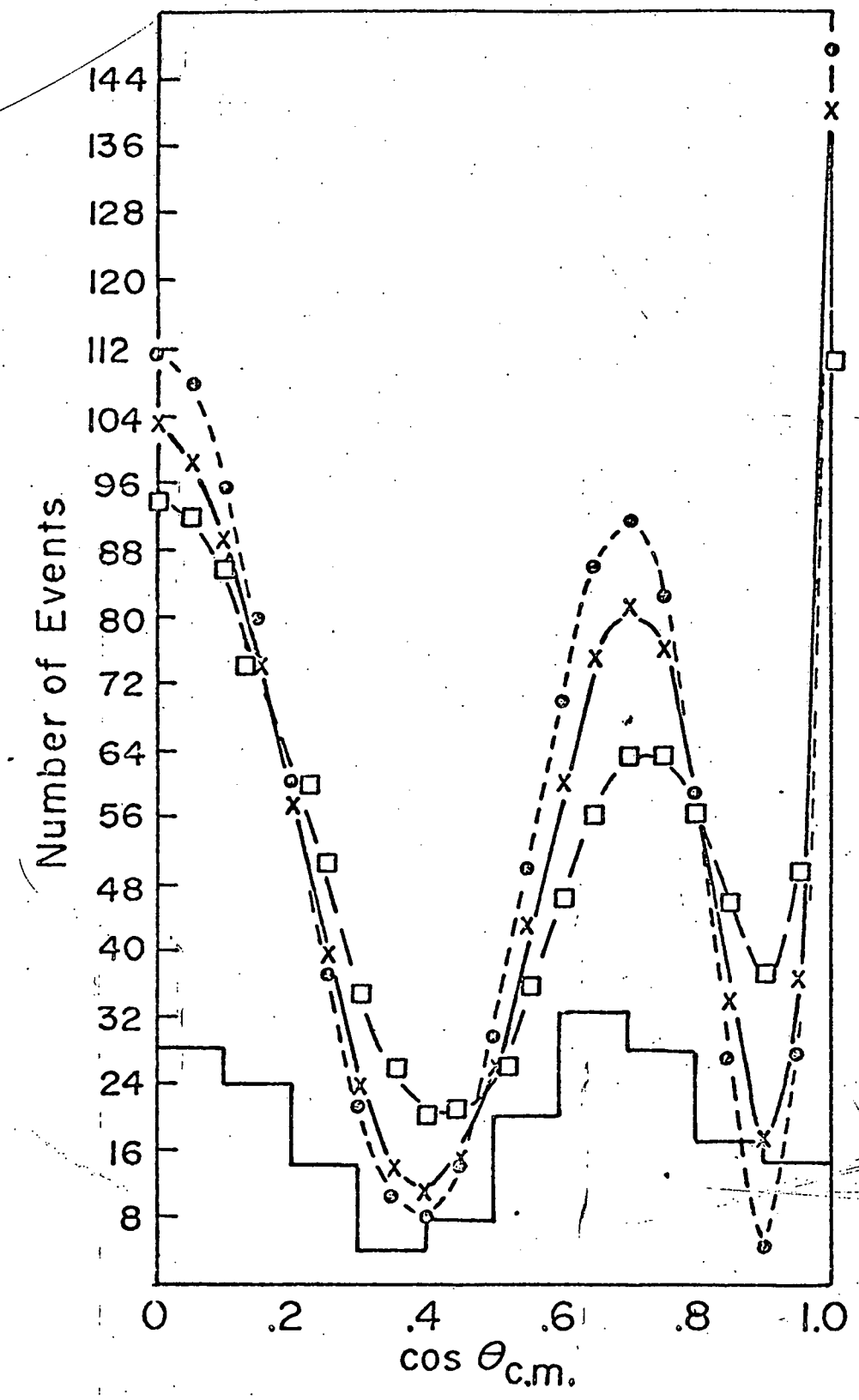


x $3\gamma + 4\gamma$ Parents Co = 520.6 ± 37.9 Prob ($X^2$) = .55

• $4\gamma$ Parents Co = 540.6 ± 49.8 Prob ($X^2$) = .50

□ $3\gamma$ Parents Co = 519.6 ± 60.0 Prob ($X^2$) = .50

# $\pi^0\eta^0$ Folded Angular Distribution
## 1.752 GeV/c

$$\frac{d\sigma}{d\Omega} = (2.25 \pm .26)\, P_0 + (1.16 \pm .66)\, P_2 + (3.1 \pm .85)\, P_4 \ \mu b/sr$$

Prob $(\chi^2) = 20\%$

$$\sigma_{\pi\eta} = 28.3 \pm 3.2\ \mu b = 4\pi a_0$$

(includes ~10% background)

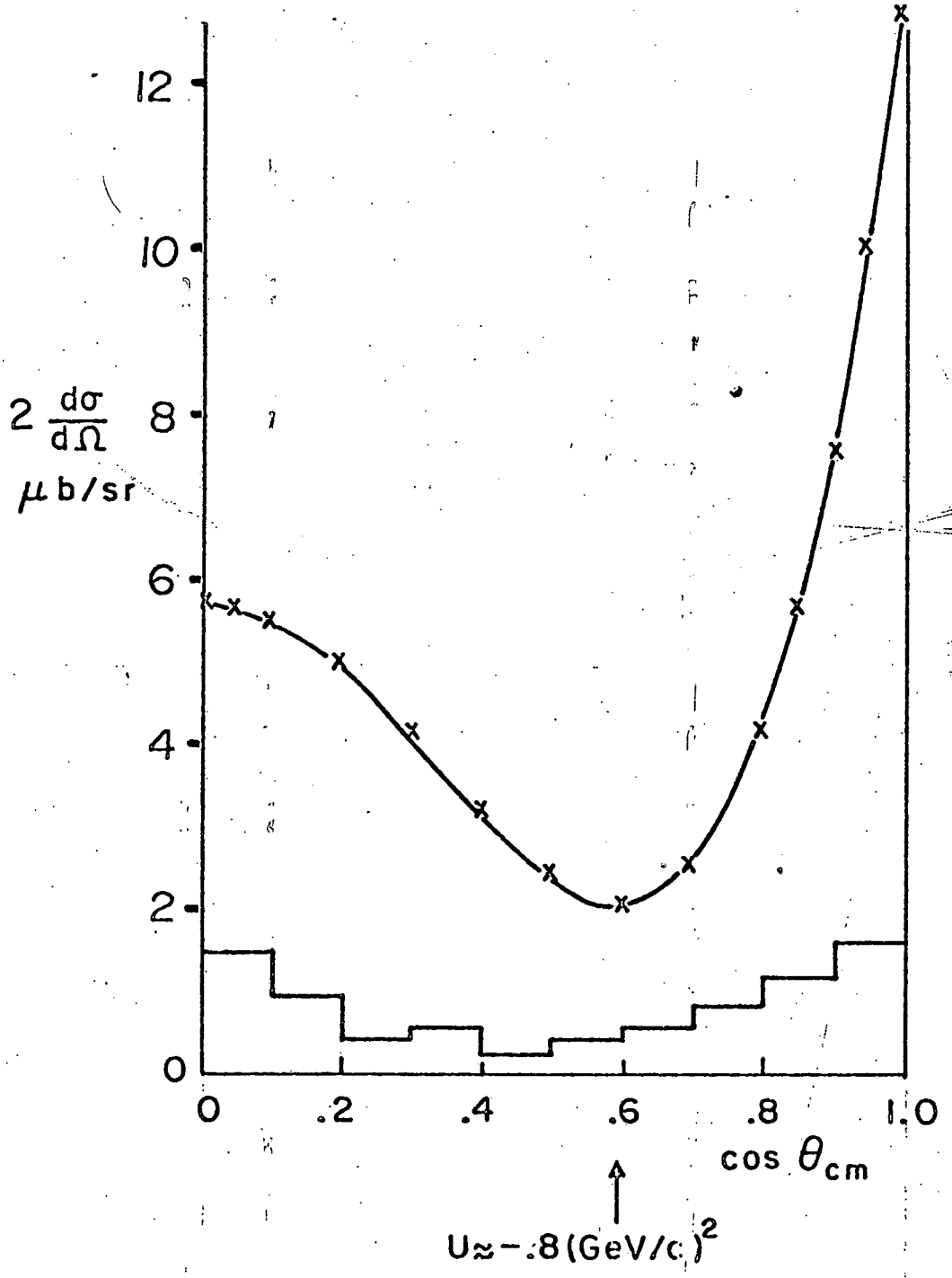

Figure 14

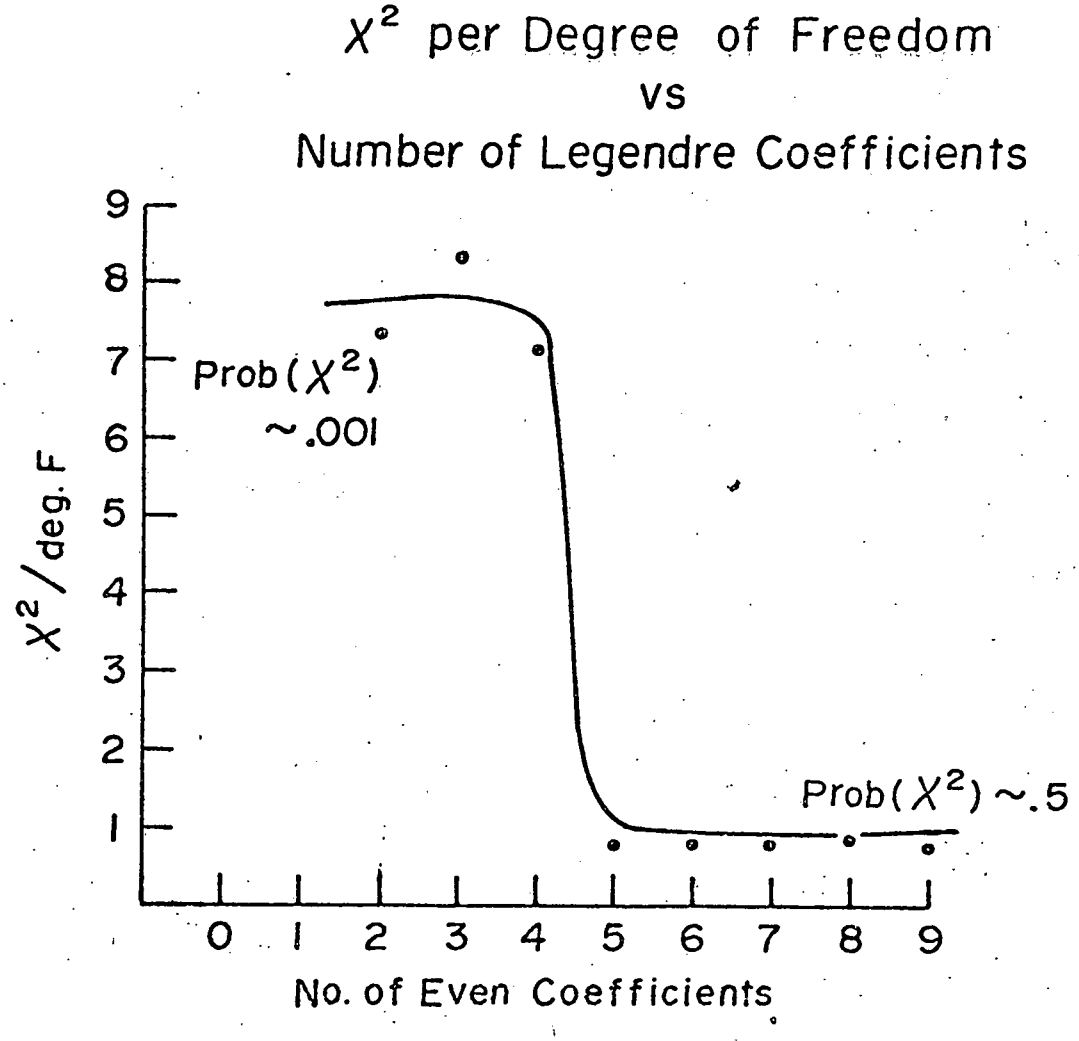
$X^2$ per Degree of Freedom
vs
Number of Legendre Coefficients
$X^2$/deg. F
9
8
7
6
5
4
3
2
1
Prob($X^2$) ~.001
Prob($X^2$) ~.5
0 1 2 3 4 5 6 7 8 9
No. of Even Coefficients

Isotopic Spin Decomposition of $\pi^+\pi^-$ Angular Distribution
1.75 GeV/c

—— $\frac{d\sigma^{+-}}{d\Omega}(I=0) = \pi^0\pi^0$ --- $\frac{d\sigma^{+-}}{d\Omega}(I=1) = (\pi^+\pi^- - \pi^0\pi^0)_{even}$

$\sigma(\bar{p}p \to \pi\pi)_0 = 38.6\,\mu b$

$\sigma(\bar{p}p \to \pi\pi)_1 = 72.9\,\mu b$

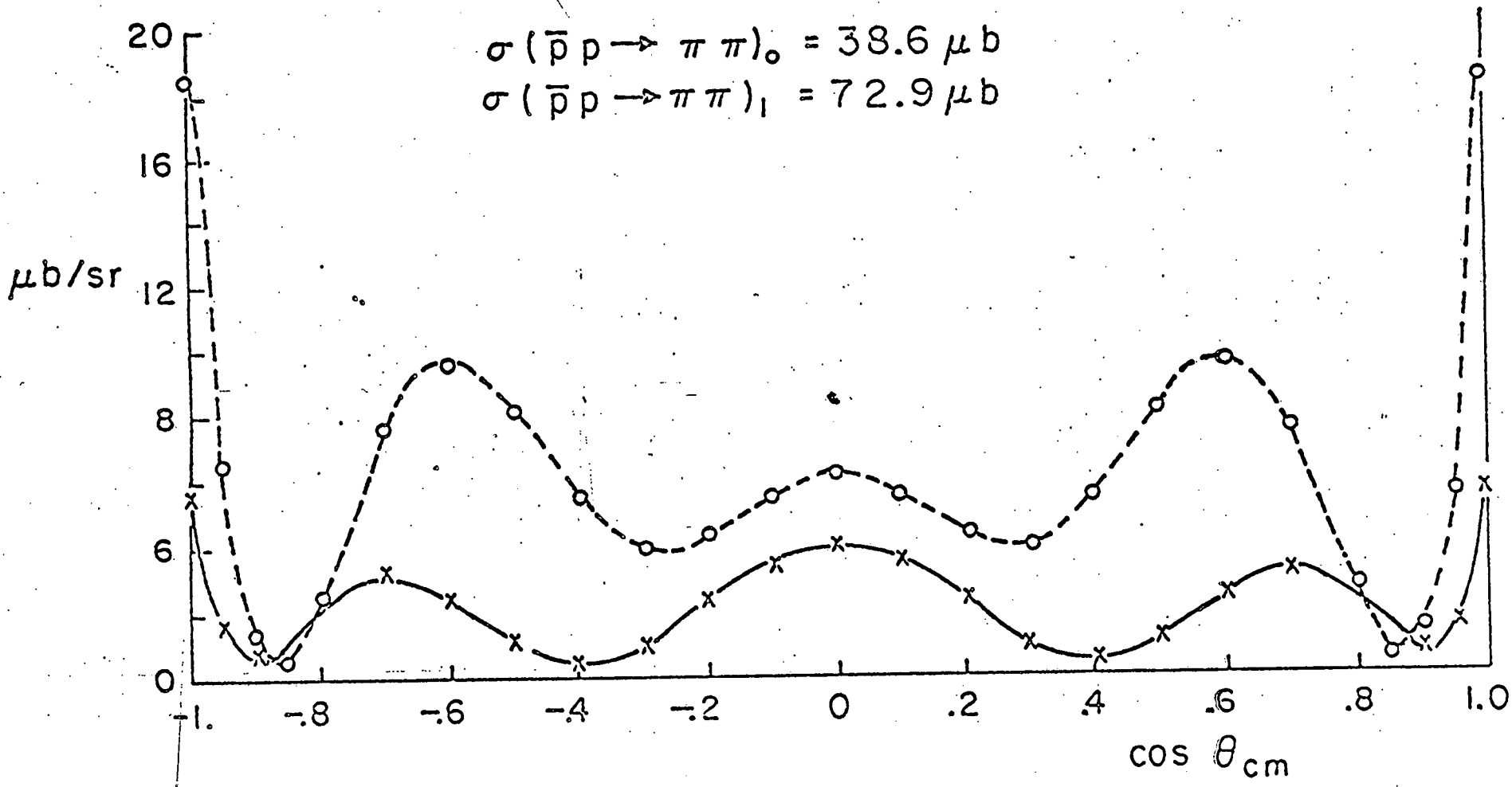

Figure 16

Raw Angular Distribution by Hodoscope